Understanding the Physics of Water Rockets Using Wireless Sensors

Eunice E. Yang
University of Pittsburgh at Johnstown
eyang@pitt.edu

Brian L. Houston
University of Pittsburgh at Johnstown
bhouston@pitt.edu

Abstract

Water rocketry is inherently a hands-on activity. Its practical nature has the advantage of engaging students, thus encouraging undergraduate students to explore and learn general physics concepts. Concepts from physics, statics, and fluid dynamics are needed to develop a system of ordinary differential equations that describe the motion of the rocket. Theoretical predictions are obtained by numerically solving the rocket's equations of motion using Euler's forward difference method.

For this particular study, water rockets were fabricated using 2-liter soda bottles to investigate the effect of varied fin configuration on kinematic performance, with very minimal change in size and mass. Data was obtained from a wireless sensor that included an altimeter and a 3-axis accelerometer to measure vibration. Data analysis was performed to identify and explain probable causes of the differences. Results showed that the 3-fin rocket was within -6% of the predicted maximum altitude in comparison to -10% for the 4-fin rocket under the same test conditions. In addition, the 3 fin rocket exhibited controlled flight characteristics as reflected by its lower magnitude and shorter period of its damped oscillatory behavior in comparison to the 4-fin rocket. Students applied Newton's second law, analyzed associated free-body diagrams, and utilized concept of moments to further explain the differences in flight performance.

I.   Introduction

Water rocketry is a practical and fun activity that can be utilized in a variety of undergraduate courses, including physics, fluid dynamics, and engineering measurements. The engaging nature of this approach helps students gain an appreciation for Newtonian physics, statics and fluid dynamics. While a popular activity among K-12 students, there appear to be only a handful of publications pertaining to water rocketry with theoretical treatment targeting undergraduate [1-4] and graduate [5-7] students. In these papers, flight data was acquired either using expensive high-speed cameras [8], older electronic methods [9], or a mathematical triangulation approach [5] to measure altitude. In addition, analyses were limited to the initial thrust phase during water/air expulsion, maximum altitude and distance traveled.

Advances in data acquisition, both in accuracy and cost, allow this paper to add to the existing knowledge base by acquiring altitude and vibration data for the entire flight with a cost-effective and simple to use wireless sensor to explain flight performance. Furthermore, equations of motion for a water rocket are derived and a numerical solution to the theory is presented. Directional stability of rockets is also examined. Experimental results of two rocket designs are compiled and compared to theoretical prediction of altitude, as well as a discussion of the probable cause of the differences in flight performance.

II.   Theory

A. Newton's second law

Kinetics of a water rocket can be investigated by analyzing the forces that affect rocket motion, which include forces due to aerodynamic drag, gravity, and thrust from water being expelled. Newton's second law, Bernoulli's principle, and adiabatic expansion of air concepts are used to develop the equations of motion of a water rocket.

As water is expelled from a water rocket, the thrust force it generates is given by

$$F_{Thrust} = u_{exit} \frac{dM_{\exp w}}{dt},$$

(1)

where u_{exit} is the velocity of the water at exit relative to the rocket and $dM_{\exp w}/dt$ is the mass flow rate of the expelled water.

The gravitational force is given by

$$F_{Gravity} = M_R g,$$

(2)

where M_R is equal to the mass of the rocket (including water) and is a function of time. The gravitational constant is denoted as g.

The aerodynamic drag of the rocket is given by

$$F_{Drag} = \frac{1}{2} \rho_{air} C_D A |v_R| v_R,$$

(3)

where the density of air is ρ_{air}, the drag coefficient is C_D, and A is the frontal area. The velocity is v_R and the absolute value of the velocity $|v_R|$ is necessary to account for the sign change of the velocity during descent.

An expression of the acceleration of the rocket can be obtained by substitution of these three equations into Newton's second law

$$a_R = \frac{\sum F}{M_R} = \frac{F_{Thrust} - F_{Gravity} - F_{Drag}}{M_R}. \tag{4}$$

B. Bernoulli's law and adiabatic assumption

To derive a numerical solution that predicts the kinematics of a water rocket, it is necessary to express F_{Thrust} of Eq. (4) in terms of air pressure inside the bottle. The initial value of this controlled variable to be used as a starting point for the numerical solution. To accomplish this, the mass flow rate of water term $dM_{exp\,w}/dt$ in Eq. (1), which is equivalent to the volumetric flow rate, can be expressed as

$$\frac{dM_{exp\,w}}{dt} = \rho_w \frac{dV}{dt} = \rho_w A_{exit} u_{exit} \tag{5}$$

where ρ_w is the density of the water, dV/dt is the volumetric flow rate, and A_{exit} is the cross sectional area across which the water expels.

Next, u_{exit} is expressed as a function of air pressure by using Bernoulli's principle given by

$$P_{air,1} + \frac{1}{2}\rho_{w,1} v_1^2 + \rho g h_1 = P_{air,2} + \frac{1}{2}\rho_{w,2} v_2^2 + \rho_{w,2} g h_2 \tag{6}$$

where location 1 is considered to be at the water and air interface inside the bottle and location 2 is at the exit (reference Fig. 1). Variables P, ρ, v, and h are internal air pressure, density of water, velocity of water, and height of water, respectively, at locations 1 and 2. Bernoulli's equation is simplified by approximating of $\rho g h_1 \approx \rho g h_2$ and $v_1 \ll v_2$. In addition, when changes in notations are made where $P_{air,1} = P_{air\,inside}$, $P_{air,2} = P_{exit}$, and $v_2 = u_{exit}$ Bernoulli's principle to reduces to

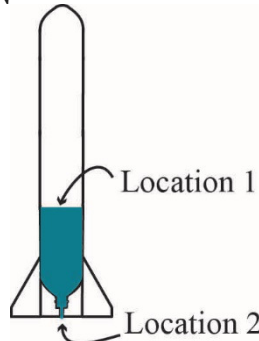$$u_{exit} = \sqrt{\frac{2(P_{air\,inside} - P_{exit})}{\rho_w}}. \tag{7}$$

Fig. 1. Locations 1 and 2 as referenced in Bernoulli's principle (Eq. (6)).

An expression for $dM_{exp\,w}/dt$ can be obtained by substitution of Eq. (7) into Eq. (5). The resulting expression can then be substituted into Eq. (1) to yield F_{Thrust} as a function of pressure

$$F_{Thrust} = 2(P_{air\,inside} - P_{exit})A_{exit} \tag{8}$$

Substitution of this new F_{Thrust} expression, gravitational force Eq. (3), and aerodynamic drag force Eq. (2) into Newton's second law Eq. (4) yields

$$a_R = \frac{2(P_{air\ inside} - P_{exit})A_{exit} - \frac{1}{2}\rho_{air}C_D A|v_R|v_R - M_R g}{M_R}. \tag{9}$$

The changes in altitude y_R and velocity v_R of the rocket are respectively sgiven by

$$dy_R = v_R dt \tag{10}$$

and

$$dv_R = a_R dt. \tag{11}$$

Eqs. (9-11) are the kinematic equations that describe the motion of the water rocket and numerical solutions can be obtained using Euler's method of forward time differentiation using $\Delta t = 0.001$ second time steps [10, 11].

C. Weather vaning

At launch rockets have a tendency to rotate about their center of gravity (Cg) in the presence of crosswinds. Consider rockets A and B (reference Fig. 2) which are launched with initial speeds of v_{oA} and v_{oB}, respectively. Allow the velocities of the air moving over the rocket to be $\bar{v}_{oA}$ and $\bar{v}_{oB}$. If each rocket is subjected to crosswind $\bar{v}_{cw}$, then by vector addition, the resultant vectors $\bar{v}_{RA}$ and $\bar{v}_{RB}$ act at angles about the y-axis of each rocket as shown. This causes each rocket to rotate to an angle of attack α as shown in Fig. 2 with $\alpha_A < \alpha_B$ due to the fact that $\bar{v}_{oA} > \bar{v}_{oB}$. This rotation is also known as weather vaning, and ultimately affects the directional stability of the rocket.
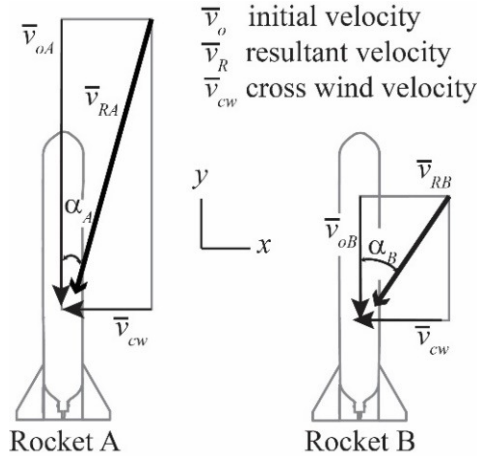

Fig. 2. Initial velocity of the rocket and crosswind velocity affects the degree at which the rocket will turn (or weather vane) into the wind at an angle of attack α.

D. Static directional stability

If the rocket is designed to be stable then the angle of attack will minimize through a series of oscillations that eventually dampen [12]. The degree of the oscillations is a function of the magnitude and locations of two net forces, $F_{net\ Cg}$ and $F_{net\ Cp}$ (reference Fig. 3a) which act at the center of gravity (⦾) and the center of pressure (⦿), respectively. The net force $F_{net\ Cg}$ is the sum of $F_{Gravity}$, F_{Drag}, and F_{Thrust} and affects translation. $F_{net\ Cp}$ is the net pressure force due to air pressure field about the body of the rocket and affects rotation. When no crosswind exists (reference Fig. 3b), the force resulting from the net pressure is zero, and the rocket assumes an ideal vertical trajectory.

The more realistic case is shown in Fig. 3c where in the presence of crosswind the net pressure force $F_{net\ Cp}$ generates a moment about Cg (⦾). The rocket rotates counterclockwise

to an angle of attack of $-\alpha$ as shown in Fig. 3d. For a stable rocket, it will go through a series of oscillations in the pitch/yaw directions and eventually dampen. An undesirable situation arises when Cp (⊙) is ahead of Cg (◉) as shown in Fig. 3e. The moment created by the net pressure force $F_{net\ Cp}$ about Cg causes the rocket to rotate clockwise. This can result in an increase in the angle of attack that is too large for the forces to minimize α, and can cause the rocket to assume an erratic/unstable flight pattern. Thus, directional stability is affected by the magnitude of the net pressure force $F_{net\ Cp}$ and its moment arm (i.e. the distance between Cp and Cg).
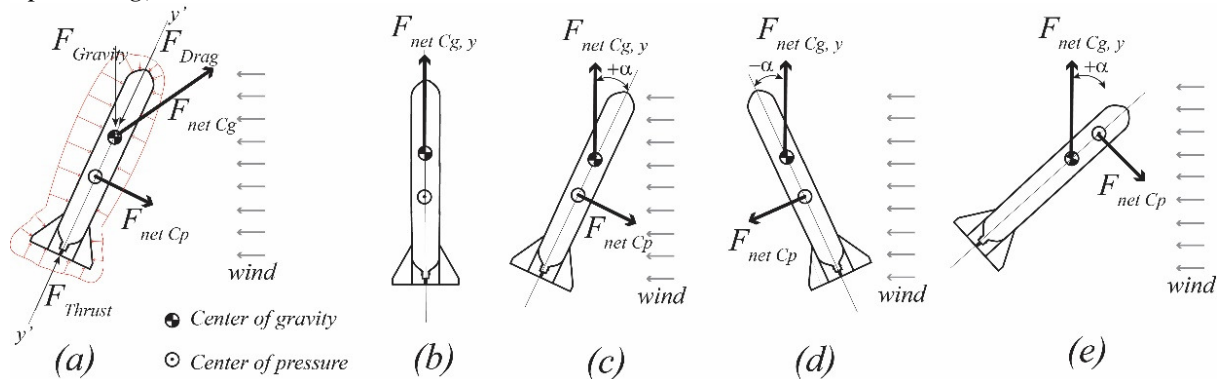

Fig. 3. (a) Free-body diagram of a rocket during flight. (b) Ideal case of rocket launch when no crosswind is present. (c-d) The rocket rotates about its Cg (◉) due to $F_{net\ Cp}$. (e) When Cp (⊙) is ahead of Cg (◉) the moment due to $F_{net\ Cp}$ can cause the rocket to undesirably rotate in a clockwise direction.

E. Net pressure force

A method to mathematically locate the center of pressure distance $\bar{Y}_{Cp}$ of a subsonic rocket was first presented by Barrowman [13, 14] under the following assumptions:

- flying at low α;
- axisymmetric and rigid body;
- steady and non-rotational flow around the body;
- nose with a sharp point; and
- fins modeled as flat plates.

Barrowman's equations can be modified to express $\bar{Y}_{Cp}$ as a function of α [15, 16]. The modified Barrowman's equations to determine $\bar{Y}_{Cp}(\alpha)$ are repeated here for convenience and will be used to understand the static directional stability of the rocket in the discussion section of this manuscript.

Dividing the rocket into three distinct sections (i.e., nose, body, and fins),the net pressure force N_i that acts at the centroid $\bar{y}_i$ (reference Fig. 4a) of each section is given by

$$N_i = (C_{N\alpha})_i \frac{1}{2}\rho_{air}v^2\alpha A_{rR} \tag{12}$$

where v is the velocity of air moving over the rocket, α is the angle of attack in radians, and A_r is the cross sectional area of the rocket's body. The parenthetical term $(C_{N\alpha})_i$ is called the shape coefficient and directly affects the magnitude of N_i. The location of the rocket's Cp can be determined by summing the moment of each N_i about the nose tip and equating it to the total moment of the rocket

$$\sum N_i \bar{y}_i = \sum (C_{N\alpha})_i \bar{Y}_{Cp}. \tag{13}$$

Solving for $\bar{Y}_{Cp}$ yields

$$\bar{Y}_{Cp} = \frac{\sum N_i \bar{y}_i}{\sum (C_{N\alpha})_i}. \tag{14}$$

The expressions for the shape coefficients for the nose (*n*), body (*B*), and fin in the presence of the body (*fb*) are defined respectively as [13, 16]

$$(C_{N\alpha})_n = 2\alpha \quad \text{(conical or parabolic nose)}, \tag{15}$$

$$(C_{N\alpha})_B = \frac{K A_B}{A_{ref}} \alpha^2, \tag{16}$$

and

$$(C_{N\alpha})_{fB} = \left(1 + \frac{R}{R+S}\right) \frac{4n \left(\frac{S}{2R}\right)^2}{1 + \sqrt{1 + \left(\frac{2l}{a+b}\right)^2}} \alpha. \tag{17}$$

The variables *a*, *b*, *l*, *R*, and *S* are related to the geometry of the fin as shown in Fig. 4b. Substitution of Eqs. (15) thru (17) into Eq. (14) yields the desired location of the center of pressure $\bar{Y}_{Cp}$ as a function of α.
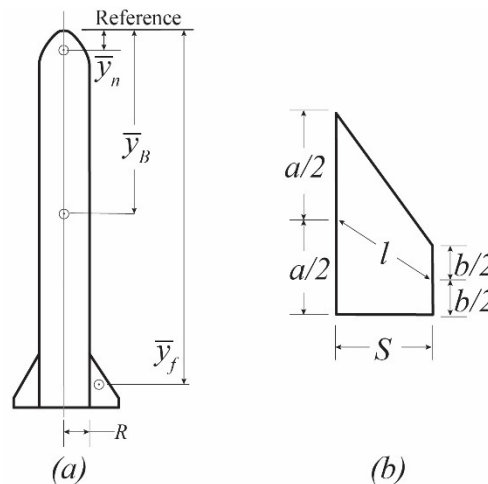

Fig. 4. (a) Geometry of the rocket and centroids of each part. Centroids of the nose, body, and fins are designated by $\bar{y}_n$, $\bar{y}_B$, and $\bar{y}_f$, respectively. (b) Geometry of fin.

III. Fabrication of water rocket

Fig. 5a depicts a water rocket fabricated using 2-liter soda bottles. The cavity just below the nose cone housed the wireless sensor in protective foam, and a recovery parachute. The body was lengthened using another bottle which was attached to the main chamber with epoxy. Interchangeable fin assemblies with 3- and 4- fins were made using 3.175 mm thick corrugated plastic. The length of the nose cone was 110 mm and the body was 553 mm in length with *R*=55.7 mm. Dimensions *a*, *b*, *l*, and *S* as identified in Fig. 4b were 140, 35, 78, and 70 mm, respectively.
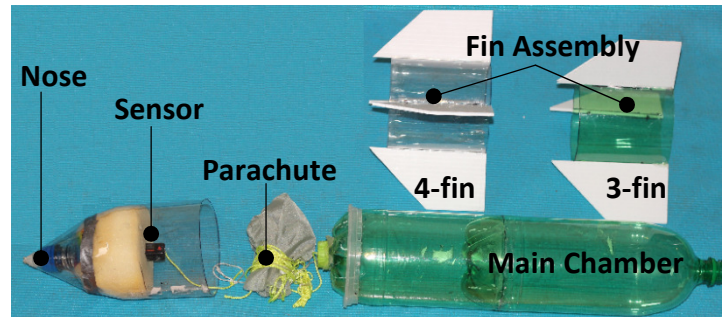
Fig. 5. Water rocket fabricated using 2L soda bottles.

The rocket launcher was made using various 12.7 mm diameter brass pipe fittings (reference Fig. 6). It was equipped with a pressure gage, pressure relief value, check valve to control the direction of air flow, and an adapter for connection to an air compressor or bicycle pump. For brevity, the reader is directed to the many available web resources that outline how to fabricate water rocket launchers.
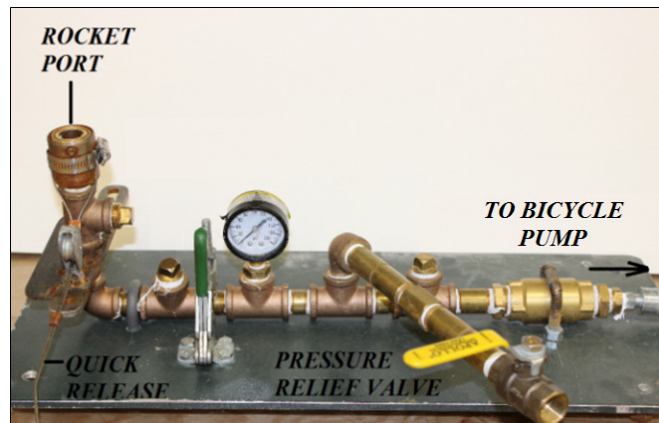

Fig. 6. Water rocket launcher.

A stand-alone wireless Bluetooth® sensor [17] equipped with an on-board data acquisition system was used to measure altitude at a rate of 20 Hz and acceleration about 3-axes at a rate of 200 Hz. The size of the sensor measured 49mm x 18mm x 14.5mm and can be recharged using a USB cord. The total mass of the sensor and batteries was 10.5 g. The manufacturer's application installed on a smart device (smartphone and iPad®) was used to view a graphical plot of the flight data immediately after each flight, as well as transmitting a CSV spreadsheet file wirelessly to an email account and/or to a cloud storage for later analysis.

IV.   Results and Discussions

A. Physical properties and flight conditions

Rockets were launched at an elevation of 696 m. The temperature was approximately 15.6 ^{o}C with an average of 3.5 m/s crosswind [18]. The 2L bottle that housed the water had a total volume (V_{bottle}) of 0.0028 m^3, body diameter d_{bottle} of 111.5 mm, and water discharge area A_{exit} of 113 mm^2. The main chamber was filled with 0.8L of water and pressurized between 30-70 psi for all flights. The physical properties of the rocket, air and water are shown in Table I.

Table I. Physical values air, water, and atmospheric conditions.

	$\bar{Y}_{Cp}$ mm	$\bar{Y}_{Cg}$ mm	M_R (g)	ρ_{air} kg/m^3	ρ_w kg/m^3	P_{exit} kPa
3- Fin	400	295	238	1.225	1000	101
4- Fin	411	300	246			

B. Flight performance

Visual observations indicated that all rockets flew vertically upward and then arced to make a descent. Erratic flight patterns were not visually observable for any flight. Typical outputs from the sensor consisting of altitude and total acceleration are shown in Fig. 7 for a 3-fin rocket launched using 60 psi. Several distinct phases include: pressurization, water and air expulsion, damped oscillations, and descent. As the pressurized air rushes into the main chamber, the rocket vibrates. At takeoff, the expulsion of water creates an impulse that reaches a peak total acceleration of 6.6 *g's*. After the water is completely expelled, acceleration decreases suddenly to 4.1 *g's*. The acceleration subsequently increases to 5.7 *g's* due to the expulsion of the compressed air and the loss of mass from the expelled water. At 0.7 seconds, with no remaining water or compressed air, the rocket is in free-flight. At this stage, damped oscillations are observed indicating pitch and yaw motions of the rocket as it attempts to overcome the effects of weather vaning. When oscillations have completely dampened, the rocket reaches its apogee of 23.2 m. During descent, the nose cone separates from the body. Oscillations between 2.5<*t*< 5.1 s reflect the nose cone swinging like a pendulum from the parachute as the assembly descends. A sudden spike is seen at 5.3 s as the nose cone impacts the ground with a total acceleration of 10.2 *g's*.
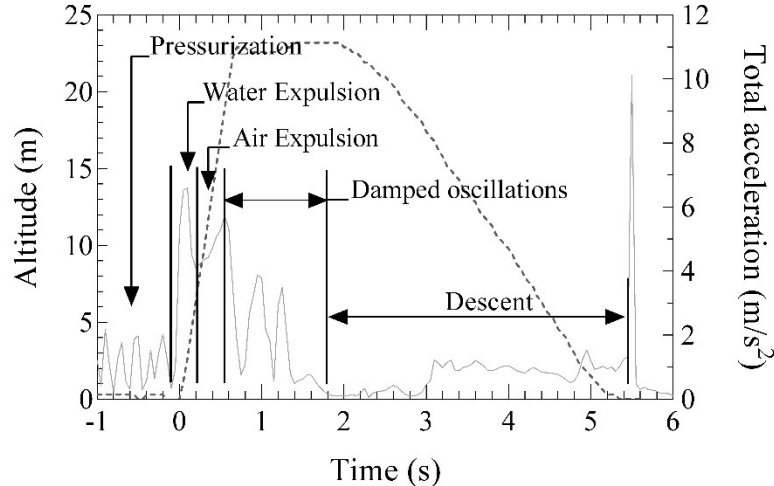

Fig. 7. 3-fin rocket pressurized to 60 psi using an initial water volume of 0.8 L.

The effect of fin configuration on flight performance was analyzed by collecting data for two fin configurations while keeping all other variables constant. Flight data from a 3-fin and 4-fin rockets using the same volume of water of 0.8 L at 60 psi are shown in Fig. 8. Since there was only a difference of eight grams between the 3-fin and 4-fin rockets, the numerical predictions for the maximum height were 24.6 m and 24.0 m, respectively. These values represent errors of -6% and -10% for the 3-fin and 4-fin rockets, respectively. Damped oscillations of each phase are compared (shaded region in Fig. 8) to examine why the

performance of the 3-fin rocket was better. Both rockets exhibit two distinct peaks in the total acceleration trace. However, the magnitudes of these peaks for the 3-fin rocket are lower (3.8 and 3.5 *g's*) and slightly shorter in duration than the 4- fin rocket (4.2 and 3.9 *g's*). This could imply that the 3-fin rocket experienced smaller pitch/yaw motions thereby indicating a better controlled flight pattern resulting in a higher altitude.

The pitch and yaw motion of the rocket is largely influenced by the magnitude of the net pressure force and the moment it creates about the *Cg*. Using Eq. (17) the fin shape coefficient of the 3-fin and 4-fin rockets were calculated to be 3.1 m and 4.1 m, respectively. This corresponds to a 25% greater net pressure force for the 4-fin rocket. The implication of this larger force is the larger moment it creates about the *Cg* causing the 4-fin rocket to experience larger oscillations in the angle of attack. The end result may have been a flight trajectory that prematurely arced, resulting in a lower altitude than predicted.
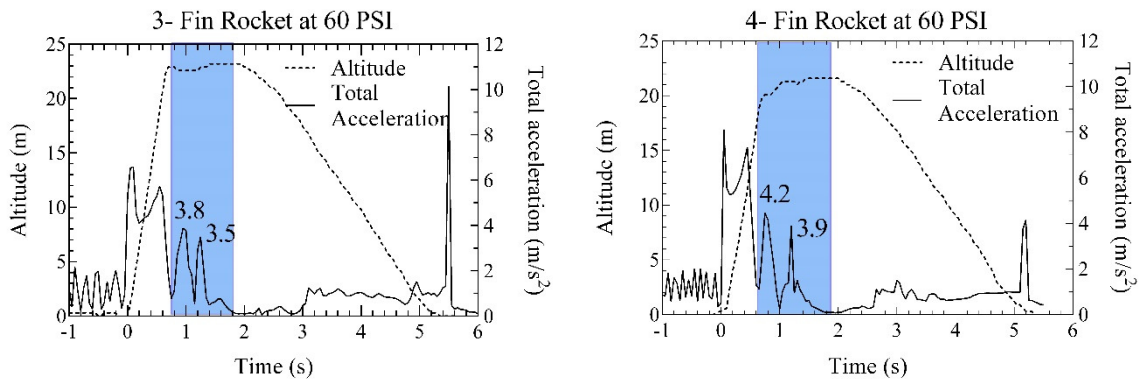

Fig. 8. Altitude and total acceleration data of 3-fin and 4-fin rockets launched using 0.8L of water at 60 psi. Differences in maximum altitude and magnitudes of the total acceleration during the damped oscillatory phase (shaded region) is noticeable.

The wireless sensor was useful in comparing differences in flight stability of the 3-fin rocket flown at a low pressure of 30 psi and a high pressure of 70 psi (reference Fig. 9). Although both flights demonstrated damped oscillations the low pressure flight required only 0.6 seconds to dampen half of a sinusoidal signal (reference Fig. 9a). For the higher pressure flight there were multiple oscillations and a total of approximately 1 second was required to reach steady state. One possible explanation is the lower initial velocity attained by the 30 psi flight caused the rocket to leave the launch pad at a larger angle of attack due to weather vaning effects as discussed in Section D. Due to its low speed, the net pressure force was probably insufficient to create a moment about the *Cg* that could quickly decrease the large angle of attack it had sustained. This resulted in less dramatic pitch/yaw movements of the rocket as indicated by the peak magnitude of the half sinusoidal cycle of 1.5 *g's* at $t=1.15$ s. For the higher pressure flight, the higher initial velocity created a net pressure force sufficient to create a moment and quickly respond to its initial angle of attack as evidenced by the multiple damped cycles with an initial peak 5.7 *g's* at $t=0.9$ s.
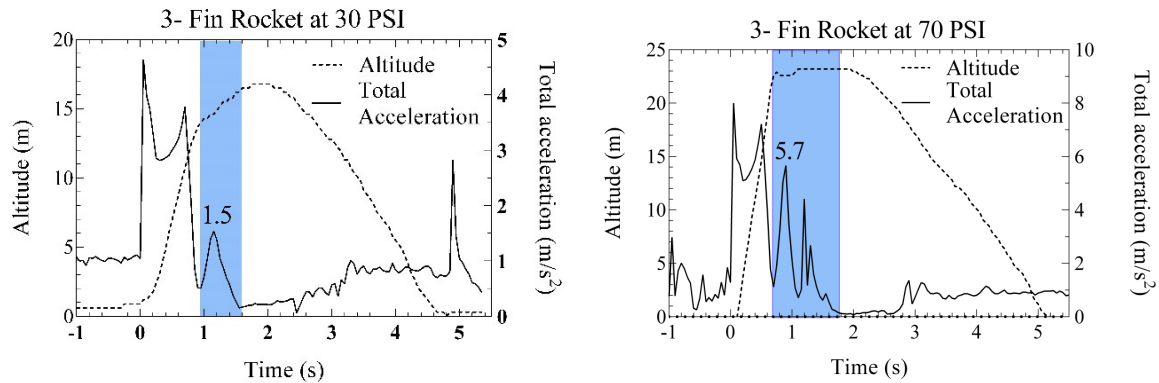
Fig. 9. Using 0.8L of water, the 3- fin rocket is launched using pressures of (a) 30 psi and (b) 70 psi. The 30 psi flight exhibits less dramatic yaw/pitch accelerations during the damped oscillation phase (shaded region) in comparison to the 70 psi flight. The peak magnitudes of the total acceleration supports this observation.

V.   Conclusion

Water rockets were fabricated from 2-liter soda bottles with three and four fin configurations. Rockets were launched using 0.8L of water at pressures ranging from 30-70 psi. A cost effective wireless sensor was used to acquire altitude and acceleration flight data. The wireless sensor data indicated the 3-fin rocket exhibited better static directional stability and resulted in a higher altitude in comparison to the 4-fin rocket under the same flight conditions. Concepts from undergraduate subjects such as dynamics, general physics, and fluid dynamics were used by students to explain the performance differences observed between the two different rocket configurations. The wireless sensor was fairly easy to use and provided opportunities for students to investigate stability of flight that would not have been possible without the sensor. While deficiencies in data acquisition are identified below, the sensor used provides a practical, low cost method of providing active learning opportunities to a large number of students. Furthermore, the use of a simple, low cost device provides an opportunity for discussing the balance between economics and accuracy in real world applications of problem solving.

Improvement to this exercise would be to address the low sampling rate of 20 Hz and large uncertainty of ± 0.25 m of the altimeter portion of the sensor. This limitation resulted in observations of false artifacts such as the plateaus in Fig. 7, Fig. 8, and Fig. 9. In addition, the true total acceleration of the rocket could have been masked due to the accelerometer's low sampling rate of 20 Hz. These issues could be resolved by using an altimeter with a higher sampling rate of 100 Hz and lower uncertainty of ± 0.1 m so that better correlation in altitude can be obtained. As for the accelerometer, a 400 Hz sampling rate would yield a resolution of 0.0025 seconds and should be sufficient to capture the desired acceleration characteristics at the onset of launch.

Future studies will include monitoring the rocket's change in angle of attack during flight using an inertial measurement unit (IMU). An IMU sensor contains both an accelerometer and a gyroscope which can allow the angle of attack during flight to be determined. Integration of an IMU sensor can range from wireless units to hard-wiring individual IMU sensors to a micro- controller such as an Arduino. Another option would be to utilize the

IMU sensor available in most modern smart phones along with an app to efficiently/cost effectively acquire the necessary data to calculate altitude, vibration, and the angle of attack during rocket flight.

Acknowledgements

References

[1]   Tomita, N., R. Watanabe, and A.V. Nebylov, *Hands-on education system using water rocket.* Acta Astronautica, 2007. **61**(11–12): p. 1116-1120.

[2].   Finney, G.A., *Analysis of a water-propelled rocket: A problem in honors physics.* Am. J. Phys., 2000. **68**(3): p. 223-227.

[3]   Thorncroft, G.E., J.R. Ridgely, and C.C. Pascual, *Hydrodynamics and thrust characteristics of a water-propelled rocket.* Int. J. of Mech. Eng. Ed., 2009. **37**(3): p. 241-261.

[4]   Kagan, D., L. Buchholtz, and L. Klein, *Soda-bottle water rockets.* Phys. Teacher., 1995. **33**: p. 150-157.

[5]   Prusa, J.M., *Hydrodynamics of a water rocket.* Society for Industrial and Applied Mathematics Review, 2000. **42**(4): p. 719-726.

[6]   Barrio-Perotti, R., et al., *Theoretical and experimental analysis of the physics of water rockets.* Eur. J. Phys., 2010. **31**: p. 1131-1147.

[7]   Gommes, C.J., *A more thorough analysis of water rockets: Moist adiabats, transient flows, and inertial forces in a soda bottle.* Am. J. Phys., 2010. **78**(3): p. 236-243.

[8]   Desbien, D.M., *High-speed video analysis in a conceptual physics class.* Phys. Teach., 2011. **49**(6): p. 332-333.

[9]   Greenwood, M.S., et al., *Using a smart-pulley Atwood machine to study rocket motion.* Am. J. Phys., 1989. **57**(10): p. 943-946.

[10]   Finney, G.A., *Analysis of a water-propelled rocket: a problem in honors physics.* American Journal of Physics [H.W.Wilson - AST], 2000. **68**(3): p. 223.

[11]   Kagan, D., *Soda-Bottle Water Rockets.* Physics Teacher, 1995. **33**(3): p. 150.

[12]   Box, S., C.M. Bishop, and H. Hunt, *Stochastic six-degree-of-freedom flight simulator for passively controlled high-power rockets.* J. Aerospace Eng., 2011. **24**(1): p. 31-45.

[13]   Barrowman, J.S. and J.A. Barrowman, *The theoretical prediction of the center of pressure*, in *Research and Development Project*. 1966, National Association of Rocketry.

[14]   Barrowman, J., *Calculating the center of pressure of a model rocket*. 1970, Centuri Engineering Company.

[15]   Galejs, R., *What Barrowman Left Out*, in *National Association of Rocketry: Sport Rocketry Technical Report*. 1999. p. 17-19.

[16]   Zarchan, P., *Tactical and strategic missile guidance*. Vol. 239 2012, Reston, Va: American Institute of Aeronautics and Astronautics.

[17]   https://www.jollylogic.com. *AltimeterThree*. 2016 [cited 2016].

[18]   Weather Underground. 2015 [cited 2015 July 8]; Available from:
        http://www.wunderground.com/history/.

Biographies

EUNICE E. YANG is currently an Associate Professor of Mechanical Engineering Technology at University of Pittsburgh at Johnstown. Her research interests include sensors, smart materials, and pedagogy. She earned her B.S. degree from University of Hawaii; an M.S. from California State University Long Beach; and, a Ph.D. in Mechanical Engineering, 2006, from Pennsylvania State University. Her background include industrial work experience in the aerospace industry while at Rockwell International, Canoga Park, CA. In addition, she has owned/managed manufacturing and software companies while residing in California. Dr. Yang may be reached at eyang@pitt.edu.

BRIAN L. HOUSTON is an Associate Professor of Civil Engineering Technology at the University of Pittsburgh at Johnstown. Prior to academia, he worked as a Senior Design Engineer in the petrochemical industry and is licensed in several states. He continues to provide structural engineering consulting services for industrial contractors and fabricators. He received a B.A. from Northwestern University in 1986, and a B.S./M.S. in Civil Engineering from Oklahoma State University in 1997/99.